

Single Production of Doubly Charged Higgsinos at linear e^-e^- colliders

Mariana Frank^{(1)†}, Katri Huitu^{(2)‡} and Santosh Kumar Rai^{(2)*}

⁽¹⁾*Department of Physics, Concordia University,*

7141 Sherbrooke St. West, Montreal, Quebec, Canada H4B 1R6

⁽²⁾ *High Energy Physics Division, Department of Physical Sciences, University of Helsinki, and Helsinki Institute of Physics, P.O. Box 64, FIN-00014 University of Helsinki, Finland*

Abstract

Several extended supersymmetric models, motivated by either grand unification, or by neutrino mass generation, predict light doubly charged higgsinos. We study the production of a single doubly charged higgsino and its decay channels at the International Linear Collider (ILC) operating in the e^-e^- mode. We analyze the production cross section for $e^-e^- \rightarrow \tilde{\Delta}_{L,R}^{\pm\pm}\chi_1^0$ as a function of different kinematic variables, followed by the decay, through several channels, of the doubly charged higgsino into a final state of two leptons plus missing energy. We include the standard model background and discuss how kinematic cuts could be used effectively to limit this background. Single production of these exotics could provide a spectacular signal for a new underlying symmetry and for physics beyond the minimal supersymmetric standard model.

PACS: 12.60.Jv, 12.60.Fr, 14.80.-j

[†]mfrank@alcor.concordia.ca

[‡]katri.huitu@helsinki.fi

*santosh.raai@helsinki.fi

1 Introduction

It is widely expected that the standard model (SM), though successful at predicting almost all experimental data in low energy physics, is not the complete theory of fundamental interactions. In addition to the theoretical inconsistencies and incompleteness of the theory, there have been recently experimental incentives to study models beyond the SM. Observations and measurements of solar and atmospheric neutrino oscillations [1], as well as indications of hot and cold dark matter [2] are not predicted, and cannot be explained, respectively, by the SM.

Supersymmetry, in the form of the minimal supersymmetric standard model (MSSM) is the most popular scenario of physics beyond the SM. It provides a satisfactory (at least qualitatively) explanation for dark matter, but suffers from the same problems as the SM when it comes to explaining neutrino masses. One must either invoke R-parity violation [3] and abandon the dark matter candidate, or add right-handed neutrinos and introduce the see-saw mechanism [4]. Supersymmetric grand unified theories (SUSY GUTs) which contain left-right supersymmetry resolve both problems naturally [5, 6]. An added bonus of SUSY GUTs is that electromagnetic, weak and strong interactions unify at the same energy scale. If such SUSY GUTs containing left-right supersymmetry are present in nature, one must devise methods to search for signals inherent in them, and absent in other models. One such signal would be the discovery of exotic particles unique to such models.

Supersymmetric left-right theories (LRSUSY), based on the product group $SU(2)_L \times SU(2)_R \times U(1)_{B-L}$, are attractive for many reasons [5, 7]. They disallow explicit R-parity breaking in the Lagrangian; they provide a natural mechanism for generating neutrino masses; and they provide a solution to the strong and weak CP problem in MSSM [8]. Neutrino masses are induced by the see-saw mechanism through the introduction of Higgs triplet fields which transform as the adjoint of the $SU(2)_R$ group and have quantum numbers $B - L = \pm 2$ (where B is baryon, and L is lepton number). While the Higgs triplet bosons are present in the non-supersymmetric version of the theory, their fermionic partners, the higgsinos, are specific to the supersymmetric version. It has been shown that, if the scale for left-right symmetry breaking is chosen so that the light neutrinos have the experimentally expected masses, these higgsinos can be light, with masses in the range of $\mathcal{O}(100)$ GeV [9]. Such particles could be produced in abundance at future colliders and thus give definite signs

of left-right symmetry at future colliders.

While the production of doubly charged Higgs bosons in the framework of the left-right model has been investigated at linear accelerators [10] and at LHC [11], the corresponding higgsinos have received less attention. The exceptions are the references in [12], where some of the properties of doubly charged higgsinos have been highlighted, and in [13], where the pair production of higgsinos in e^+e^- was analyzed. We note that doubly charged higgsinos also appear in the so-called 3-3-1 models (models based on the $SU(3)_c \times SU(3)_L \times U(1)_N$ symmetry) [14].

In this present work, we concentrate on a definite signal for doubly charged higgsinos: the production of a single one at an e^-e^- collider, followed by the decay (through several channels) to $e^-e^- + E_{\text{miss}}$. In order to obtain definite predictions for the signal, we perform our analysis in the context of the LRSUSY, though we expect the results for the 3-3-1 model to be similar. We concentrate first on the details and characteristics of the production cross section. We then discuss the possible decay modes of the doubly charged higgsinos (either two-body or three-body, depending on the spectrum characteristics). We complete our analysis with the discussion of the SM background, and indicate how cuts could be employed most efficiently to reduce these backgrounds.

Our paper is organized as follows. In Section 2 we describe the LRSUSY model, with particular emphasis on the sectors of interest, as well as summarize the restrictions on the relevant Yukawa couplings. In Section 3 we present the analysis for the production and decay, separately for the left and right-handed doubly charged higgsino and of the SM backgrounds and cuts needed to observe the signal. We reach the conclusions in Section 4. The Appendix contains the mixing in the scalar and gaugino/higgsino sectors which enter our calculation.

2 Description of the LRSUSY Model

The minimal supersymmetric left-right model is based on the gauge group $SU(3)_C \times SU(2)_L \times SU(2)_R \times U(1)_{B-L}$. The matter fields of this model consist of three families of quark and lepton chiral superfields which transform under the gauge group as:

$$Q = \begin{pmatrix} u \\ d \end{pmatrix} \sim \left(3, 2, 1, \frac{1}{3}\right), \quad Q^c = \begin{pmatrix} d^c \\ u^c \end{pmatrix} \sim \left(3^*, 1, 2, -\frac{1}{3}\right),$$

$$L = \begin{pmatrix} \nu \\ e \end{pmatrix} \sim (1, 2, 1, -1), \quad L^c = \begin{pmatrix} e^c \\ \nu^c \end{pmatrix} \sim (1, 1, 2, 1), \quad (1)$$

where the numbers in the brackets denote the quantum numbers under $SU(3)_C \times SU(2)_L \times SU(2)_R \times U(1)_{B-L}$. The Higgs sector consists of the bidoublet and triplet Higgs superfields:

$$\begin{aligned} \Phi_1 &= \begin{pmatrix} \Phi_{11}^0 & \Phi_{11}^+ \\ \Phi_{12}^- & \Phi_{12}^0 \end{pmatrix} \sim (1, 2, 2, 0), \quad \Phi_2 = \begin{pmatrix} \Phi_{21}^0 & \Phi_{21}^+ \\ \Phi_{22}^- & \Phi_{22}^0 \end{pmatrix} \sim (1, 2, 2, 0) \\ \Delta_L &= \begin{pmatrix} \frac{1}{\sqrt{2}}\Delta_L^- & \Delta_L^0 \\ \Delta_L^{--} & -\frac{1}{\sqrt{2}}\Delta_L^- \end{pmatrix} \sim (1, 3, 1, -2), \quad \delta_L = \begin{pmatrix} \frac{1}{\sqrt{2}}\delta_L^+ & \delta_L^{++} \\ \delta_L^0 & -\frac{1}{\sqrt{2}}\delta_L^+ \end{pmatrix} \sim (1, 3, 1, 2), \\ \Delta_R &= \begin{pmatrix} \frac{1}{\sqrt{2}}\Delta_R^- & \Delta_R^0 \\ \Delta_R^{--} & -\frac{1}{\sqrt{2}}\Delta_R^- \end{pmatrix} \sim (1, 1, 3, -2), \quad \delta_R = \begin{pmatrix} \frac{1}{\sqrt{2}}\delta_R^+ & \delta_R^{++} \\ \delta_R^0 & -\frac{1}{\sqrt{2}}\delta_R^+ \end{pmatrix} \sim (1, 1, 3, 2) \end{aligned} \quad (2)$$

The bi-doublet Higgs superfields Φ_1, Φ_2 break the $SU(2)_L \times U(1)_Y$ symmetry and generate a Cabibbo-Kobayashi-Maskawa mixing matrix. Supplementary Higgs representations are needed to break left-right symmetry spontaneously: triplet Higgs Δ_L, Δ_R bosons are chosen to also support the seesaw mechanism. Since the theory is supersymmetric, additional triplet superfields δ_L, δ_R are needed to cancel triangle gauge anomalies in the fermionic sector. The most general superpotential involving these superfields is:

$$\begin{aligned} W &= \mathbf{Y}_Q^{(i)} Q^T \Phi_i i\tau_2 Q^c + \mathbf{Y}_L^{(i)} L^T \Phi_i i\tau_2 L^c + i(\mathbf{h}_l L^T \tau_2 \delta_L L + \mathbf{h}_l L^c \tau_2 \Delta_R L^c) \\ &\quad + \mu_3 [Tr(\Delta_L \delta_L + \Delta_R \delta_R)] + \mu_{ij} Tr(i\tau_2 \Phi_i^T i\tau_2 \Phi_j) + W_{NR} \end{aligned} \quad (3)$$

where W_{NR} denotes (possible) non-renormalizable terms arising from higher scale physics or Planck scale effects [9]. The presence of these terms insures that, when the SUSY breaking scale is above M_{WR} , the ground state is R-parity conserving. In addition, the potential also includes F -terms, D -terms as well as soft supersymmetry breaking terms:

$$\begin{aligned} \mathcal{L}_{soft} &= [\mathbf{A}_Q^i \mathbf{Y}_Q^{(i)} \tilde{Q}^T \Phi_i i\tau_2 \tilde{Q}^c + \mathbf{A}_L^i \mathbf{Y}_L^{(i)} \tilde{L}^T \Phi_i i\tau_2 \tilde{L}^c + i\mathbf{A}_{LR} \mathbf{h}_l (\tilde{L}^T \tau_2 \delta_L \tilde{L} + \tilde{L}^c \tau_2 \Delta_R \tilde{L}^c) \\ &\quad + m_\Phi^{(ij)2} \Phi_i^\dagger \Phi_j] + [(m_L^2)_{ij} \tilde{l}_{Li}^\dagger \tilde{l}_{Lj} + (m_R^2)_{ij} \tilde{l}_{Ri}^\dagger \tilde{l}_{Rj}] - M_{LR}^2 [Tr(\Delta_R \delta_R) + Tr(\Delta_L \delta_L) + h.c.] \\ &\quad - [B\mu_{ij} \Phi_i \Phi_j + h.c.] \end{aligned} \quad (4)$$

The symmetry is broken spontaneously to $U(1)_{em}$ when the neutral Higgs fields acquire non-zero vacuum expectation values (VEV 's):

$$\langle \Phi_1 \rangle = \begin{pmatrix} \kappa_1 & 0 \\ 0 & \kappa_1' e^{i\omega_1} \end{pmatrix}, \quad \langle \Phi_2 \rangle = \begin{pmatrix} \kappa_2' e^{i\omega_2} & 0 \\ 0 & \kappa_2 \end{pmatrix}, \quad \langle \Delta_L \rangle = \begin{pmatrix} 0 & v_{\Delta_L} \\ 0 & 0 \end{pmatrix},$$

$$\langle \delta_L \rangle = \begin{pmatrix} 0 & 0 \\ v_{\delta_L} & 0 \end{pmatrix}, \quad \langle \Delta_R \rangle = \begin{pmatrix} 0 & v_{\Delta_R} \\ 0 & 0 \end{pmatrix}, \quad \langle \delta_R \rangle = \begin{pmatrix} 0 & 0 \\ v_{\delta_R} & 0 \end{pmatrix}.$$

The Lagrangians in (3) and (4) give rise to the interactions of the doubly charged higgsinos $\tilde{\Delta}_{L,R}^{--}$. As these are determined by the magnitude of the triplet Yukawa couplings, we review first the restrictions on these.

2.1 Experimental limits on triplet masses and Yukawa couplings

Indirect experimental limits for the triplet Yukawa couplings come from lepton number violating processes mediated by doubly charged Higgs bosons. These processes constrain the first two generations, while the third generation couplings remain constrained only by the requirement of perturbativity. The constraints on Yukawa couplings as a function of the doubly charged Higgs mass can be found in [15, 16] and are given as follows

$$\begin{aligned} h_{e\mu} h_{ee} &< 3.2 \times 10^{-11} \text{ GeV}^{-2} \cdot M_{\Delta^{--}}^2 \quad \text{from } \mu \rightarrow \bar{e} e e, \\ h_{e\mu} h_{\mu\mu} &< 2 \times 10^{-10} \text{ GeV}^{-2} \cdot M_{\Delta^{--}}^2 \quad \text{from } \mu \rightarrow e \gamma, \\ h_{ee}^2 &< 9.7 \times 10^{-6} \text{ GeV}^{-2} \cdot M_{\Delta^{--}}^2 \quad \text{from Bhabha scattering,} \\ h_{\mu\mu}^2 &< 2.5 \times 10^{-5} \text{ GeV}^{-2} \cdot M_{\Delta^{--}}^2 \quad \text{from } (g-2)_\mu, \\ h_{ee} h_{\mu\mu} &< 2.0 \times 10^{-7} \text{ GeV}^{-2} \cdot M_{\Delta^{--}}^2 \quad \text{from muonium - antimuonium transition.} \end{aligned}$$

Bhabha scattering indirect limits were studied also at LEP, and it was found that if $h_{ee} > 0.7$, the doubly charged Higgs mass should be in the TeV region [17, 18]. Also at LEP, direct searches of doubly charged Higgs were performed. From the pair production of doubly charged Higgses a lower bound around 100 GeV was established, if $h_{ij} > 10^{-7}$, $i, j = e, \mu, \tau$ [18, 19]. From the single production of doubly charged Higgs boson in e^+e^- collisions, couplings $h_{ee} < 0.071$ are allowed, if $M_{\Delta^{--}} < 160$ GeV, assuming 100% branching fraction to leptons [17]. At HERA the single production of doubly charged Higgs boson was studied in e^+p collisions [20] and a lower limit of 141 GeV was found on the doubly charged Higgs mass if the coupling $h_{e\mu} = 0.3$, while the mass limit for $h_{e\tau} = 0.3$ was 112 GeV. For heavier doubly charged Higgses, the corresponding Yukawa couplings are less restricted, and for $M_{\Delta^{--}} > 150$ GeV triplet Yukawa couplings are not constrained by HERA. Note that the direct search limits are the only ones which include the third generation couplings.

For simplicity we assume that the flavor-violating off-diagonal entries in the coupling matrix are zero and only the flavor diagonal elements have finite entries. Assuming that the triplet Yukawa couplings are degenerate the most stringent constraints for the $\Delta L = 2$ couplings come from results for the muonium-antimuonium transitions which depend on the mass scale for the triplet Higgs fields *viz.* $h_u \equiv \tilde{f}_u < 0.44 M_{\Delta\pm\pm} \text{ TeV}^{-1}$, at 90% C.L. [16].

We now proceed to examine the doubly charged higgsino sector of the theory. We first review the known information on their masses and couplings, then proceed to discuss their production and decay channels. For completeness, we present the information on the mixing in the chargino, neutralino and charged scalar sectors of our theory, insofar as relevant to our discussion of doubly charged higgsinos, in the Appendix.

3 Production and Decay of Doubly Charged Higgsinos

We analyze first the single production of the doubly charged higgsino at the next generation linear collider running in the e^-e^- mode. The linear collider operating in this mode will provide an ideal environment for single production of such doubly charged particles and

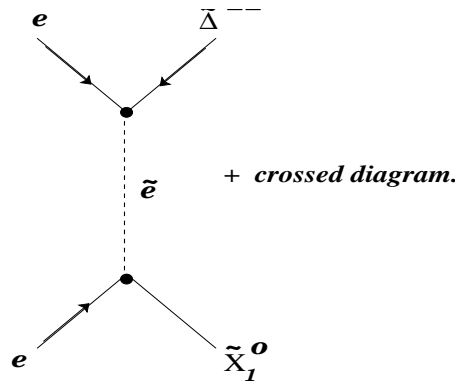


Figure 1: *Feynman graphs for the two-body production of $\tilde{\Delta}^{--}\tilde{\chi}_1^0$ at e^-e^- collider.*

signals for such processes can be remarkably free from backgrounds. We focus on a typical production mode for the doubly charged higgsinos $\tilde{\Delta}^{--}$ in association with the lightest neutralino and calculate the rates for the process:

$$e^-e^- \longrightarrow \tilde{\Delta}^{--}\tilde{\chi}_1^0 \quad (5)$$

and study the signal resulting from the decays of the $\tilde{\Delta}^{--}$. This production is mediated by the selectron exchange¹ as shown in Fig 1 and would be accompanied by large missing energy as the lightest neutralino in the final state is stable and escapes undetected. The e^-e^- production mode would allow us to probe a large range of masses of the doubly charged higgsino, compared to the case where one produces them in pairs at linear colliders operating in the e^+e^- mode. The upper value of the mass of the produced $\tilde{\Delta}^{--}$ will be constrained only

Sample point A :	$\tan \beta = 20$	$M_{\tilde{\chi}_1^0} = 91.8 \text{ GeV}$	$M_{\tilde{\chi}_2^0} = 180.6 \text{ GeV}$
$M_{B-L} = 25 \text{ GeV}$	$M_L = M_R = 250 \text{ GeV}$	$M_{\tilde{\chi}_3^0} = 250.0 \text{ GeV}$	
$\mu_1 = 1000 \text{ GeV}$	$\mu_3 = 300 \text{ GeV}$		
$v_{\Delta_L} = 1.5 \times 10^{-8} \text{ GeV}$	$v_{\delta_L} = 1.0 \times 10^{-8} \text{ GeV}$	$M_{\tilde{\chi}_1^\pm} = 249.0 \text{ GeV}$	$M_{\tilde{\chi}_2^\pm} = 300.0 \text{ GeV}$
$v_{\Delta_R} = 3000 \text{ GeV}$	$v_{\delta_R} = 1000 \text{ GeV}$	$M_{\tilde{\chi}_3^\pm} = 911.7 \text{ GeV}$	
Sample point B :	$\tan \beta = 30$	$M_{\tilde{\chi}_1^0} = 217.3 \text{ GeV}$	$M_{\tilde{\chi}_2^0} = 441.7 \text{ GeV}$
$M_{B-L} = 100 \text{ GeV}$	$M_L = M_R = 500 \text{ GeV}$	$M_{\tilde{\chi}_3^0} = 450.0 \text{ GeV}$	
$\mu_1 = 500 \text{ GeV}$	$\mu_3 = 500 \text{ GeV}$		
$v_{\Delta_L} = 1.5 \times 10^{-8} \text{ GeV}$	$v_{\delta_L} = 1.0 \times 10^{-8} \text{ GeV}$	$M_{\tilde{\chi}_1^\pm} = 447.8 \text{ GeV}$	$M_{\tilde{\chi}_2^\pm} = 500.0 \text{ GeV}$
$v_{\Delta_R} = 2500 \text{ GeV}$	$v_{\delta_R} = 1500 \text{ GeV}$	$M_{\tilde{\chi}_3^\pm} = 500 \text{ GeV}$	

Table 1: *Sample points of the particle spectrum. The left column contains the input values for the parameters of the model, while the right column lists the masses of the lightest the neutralinos and charginos corresponding to the choice of input parameters.*

by the mass of the lightest neutralino and the kinematic threshold of the machine energy of the collider. In the latter part of this section we will focus on the possible signatures for different final states.

For the analysis, we choose two representative points in the parameter space of the model as presented in Table 1 (we have consistently chosen negligibly small values for the VEV's v_{Δ_L} and v_{δ_L} so that the constraints on the ρ -parameter is not disturbed). This will lead, as our discussions will show, to clear signals for doubly charged higgsino production. Moreover,

¹We neglect the contribution coming from the exchange of doubly charged Higgs (Δ) in the s-channel which we find to be negligibly small in comparison. This is because of the huge suppression coming from the mass of Δ in the propagator, which we have assumed to be large.

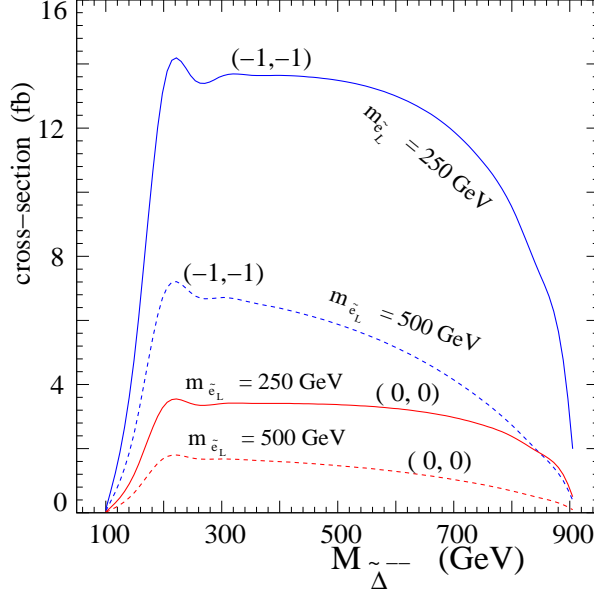


Figure 2: The production cross section as a function of the triplet higgsino mass for $\sqrt{s} = 1$ TeV. We highlight the dependence of the production cross section (for $\tilde{\Delta}_L^{--}$) on the beam polarization $(-1, -1)$ as compared with the unpolarized cross sections for two choices of selectron mass (250 GeV and 500 GeV). The plot is produced for the sample point **A** given in Table 1.

a reasonable choice for the $\Delta L = 2$ couplings leads to like-sign lepton signals which can have very suppressed or no SM background. For simplicity, we have however focused only on the diagonal $\Delta L = 2$ couplings. As one could produce both the left or right-chiral states of $\tilde{\Delta}^{--}$, we divide this section into two parts and discuss the production of the two chiral states separately.

3.1 The left-handed higgsino $\tilde{\Delta}_L^{--}$

3.1.1 Production

In Fig. 2 we plot the production cross sections of $\tilde{\Delta}_L^{--}$ with both unpolarized and polarized e^- beams. The center-of-mass energy is taken to be $\sqrt{s} = 1$ TeV². We choose a coupling strength of $\tilde{f}_{ee} = 0.1$, in agreement with bounds on $\Delta L = 2$ couplings from different experimental data as listed in section 2.1. With masses for the triplet Higgs fields in the TeV-range one

²While the initial center-of-mass energy at the ILC [21] is expected to be $\sqrt{s} = 500$ GeV, it is likely to be increased soon to 1 TeV, for which more promising signals can be observed.

can easily obtain larger values for the couplings. In contrast to existing bounds on the mass of the triplet Higgs (quite severe for larger values of the $\Delta L = 2$ couplings), the mass of $\tilde{\Delta}_L^{--}$ is not strongly constrained ($\gtrsim 100$ GeV). So a light $\tilde{\Delta}_L^{--}$ with a large $\Delta L = 2$ coupling is not ruled out and remains consistent with experimental data. In the sample points given in Table 1 the lightest neutralino is the lightest supersymmetric particle (LSP). We have used *sample point A* in calculating the rates in Fig. 2.

The production cross sections are shown for two different choices of selectron mass *viz.* 250 GeV and 500 GeV. As expected, the larger value of the selectron mass in the propagator suppresses the production cross section. The production is however enhanced by a factor of four for the left-chiral $\tilde{\Delta}_L^{--}$, if one uses 100% left-polarization for both beams, as shown in Fig 2. Other combinations make the production cross section vanish for the left-chiral state because of the $(1 - \gamma_5)$ coupling (see Section 5.4). The figure shows that even with a conservative value for the $\Delta L = 2$ coupling, one expects a production cross section between 10-14 fb for polarized beams and a 250 GeV-mass selectron. With an integrated luminosity of 500 fb^{-1} one can have a large production rate of the doubly charged higgsino $\tilde{\Delta}_L^{--}$.

It is worth noting that the choice of the soft parameters have a role to play in the production mechanism, as they form the basic entries in the matrix diagonalizing the neutralino mass matrix (see Section 5.2). The $e - \tilde{e} - \tilde{\chi}^0$ coupling, which can be written down as

$$\ell^- \tilde{\ell}_L \chi_k^0 \rightarrow \frac{1}{\sqrt{2}}(g_L N_{k1} + g_V N_{k3})P_L$$

and the components of the lightest neutralino mass eigenstate will thus be modified for different choices of the soft parameters in the theory. A quick look at Table 1 shows that the mass splitting between the lightest neutralino and the next lightest neutralino strongly depends on the ratio $\frac{v_{\Delta R}}{v_{\delta R}}$ where a larger ratio results in smaller mass splitting. This can lead to interesting signatures where the next lightest neutralino can become the next-lightest SUSY particle (NLSP). Such interesting spectrum analysis is however left for future work and not considered here anymore. We show the dependence of the relevant soft parameters on the lightest neutralino mass and the corresponding production cross sections in Fig. 3 and Fig. 4. The mass of the doubly-charged higgsino is $M_{\tilde{\Delta}_L^{--}} = \mu_3$, with the exchanged selectron mass fixed at $m_{\tilde{e}_L} = 500$ GeV while the polarization choice for the colliding electron beams is (-1,-1) which maximizes the production cross section for the left-handed higgsino. In Fig. 3(a), we show the lightest neutralino mass as a function of the $U(1)_{B-L}$ gaugino

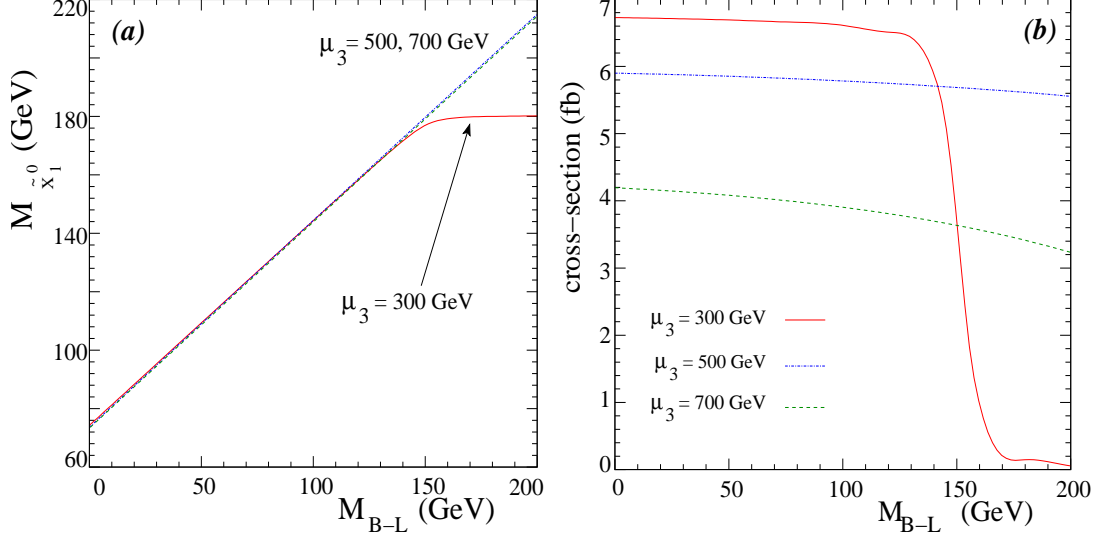


Figure 3: (a) The lightest neutralino mass as a function of M_{B-L} . (b) The production cross section as a function of M_{B-L} , for three different values of μ_3 . The other parameters are matched with the remaining inputs to sample point **A** given in Table 1. Here $\sqrt{s} = 1$ TeV, $m_{\tilde{e}_L} = 500$ GeV and $M_{\tilde{\Delta}_L^{--}} = \mu_3$.

mass parameter M_{B-L} for three different values of μ_3 . We find that, increasing value of M_{B-L} (the other model parameters fixed to values for *sample point A* given in Table 1), the lightest neutralino state becomes heavier. In fact the lightest neutralino mass shows no dependence on μ_3 for low values of M_{B-L} , but can be seen to admit a dominant admixture of the right higgsino state beyond $M_{B-L} \sim 140$ GeV for the lower choice of $\mu_3 = 300$ GeV. This fact is highlighted in the plot for the cross section, which starts falling rapidly for values of $M_{B-L} \geq 140$ GeV as shown in Fig. 3(b), for $\mu_3 = 300$ GeV. For large M_{B-L} , the lightest state contains a dominant admixture of the right higgsino states and thus its coupling strength is decreased. The cross section for the other choices of $\mu_3 = 500$ GeV and 700 GeV do not show the sharp fall as the lightest neutralino remains dominantly $U(1)_{B-L}$ -gaugino-like for the choice of M_{B-L} in the plots.

In Fig. 4(a) we plot the lightest neutralino mass as a function of $M_L = M_R = M_2$ for the three different values of μ_3 . The mass of $\tilde{\chi}_1^0$ again shows little dependence on μ_3 for low values of M_2 . The contribution of the right higgsino state in the lightest neutralino shows up early for the lower values of μ_3 as seen in Fig. 4(a). As shown in Fig. 4(b), in contrast to Fig. 3(b), the cross section varies over a larger value when increasing the value of the

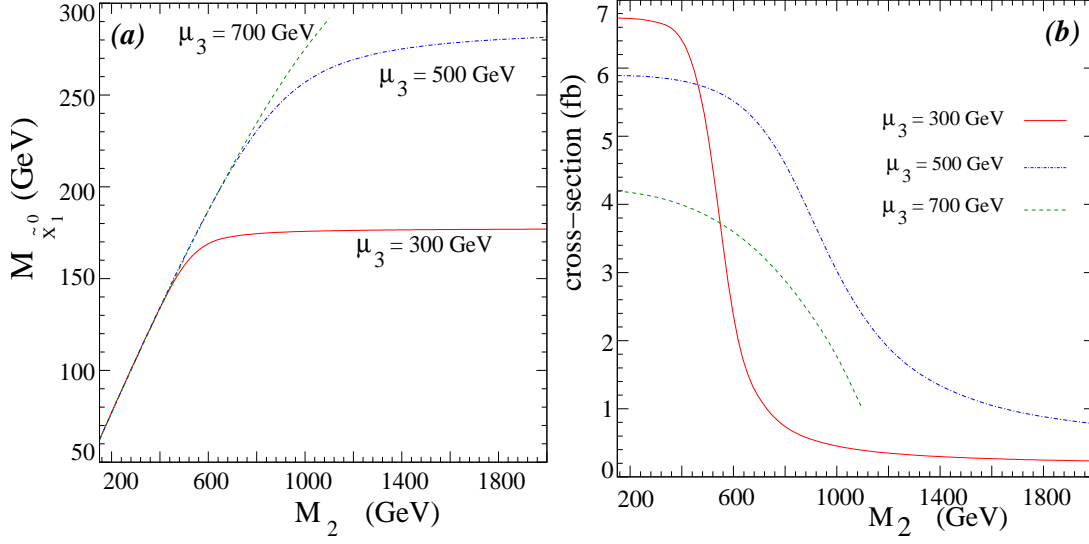


Figure 4: (a) The lightest neutralino mass as a function of $M_L = M_R = M_2$. (b) The production cross section as a function of M_2 , for three different values of μ_3 . The other parameters are matched with the remaining inputs to sample point **A** given in Table 1. Here $\sqrt{s} = 1$ TeV, $m_{\tilde{e}_L} = 500$ GeV and $M_{\tilde{\Delta}_L^{--}} = \mu_3$.

neutralino mass (increasing value of the soft parameter). The cross section is again seen to show a sharp fall at different values of M_2 for different choices of μ_3 . This is again due to the increase of the right-higgsino component in the lightest neutralino and the corresponding change in the values of the $e - \tilde{e}_L - \tilde{\chi}_1^0$ coupling. The curves for $\mu_3 = 700$ GeV end abruptly, because the cross section becomes zero as the lightest neutralino mass becomes greater than 300 GeV and the process is kinematically disallowed at the $\sqrt{s} = 1$ TeV machine.

We now proceed to perform the signal analysis for the $\tilde{\Delta}_L^{--}$ production in detail.

3.1.2 Decays

We focus on the event rates for specific final states arising through the decay of the left-chiral doubly charged higgsino. This would require the knowledge of all possible decay modes accessible to the $\tilde{\Delta}^{--}$. In general, the following 2-body decays of the doubly charged higgsinos are allowed:

- $\tilde{\Delta}^{--} \rightarrow \tilde{\ell}^- \ell^-$,
- $\tilde{\Delta}^{--} \rightarrow \Delta^{--} \tilde{\chi}_i^0$,

- $\tilde{\Delta}^{--} \longrightarrow \tilde{\chi}_i^- \Delta^-$.

However, we assume the triplet Higgses to be heavier (which allows a less constrained $\Delta L = 2$ coupling), and degenerate in mass, which renders them kinematically inaccessible for decay modes of the relatively lighter doubly charged higgsinos. Hence, we concentrate on the only favored channel for decay which is $\tilde{\Delta}^{--} \longrightarrow \tilde{\ell}^- \ell^-$, provided $m_{\tilde{\ell}} < M_{\tilde{\Delta}^{--}}$. For relatively light higgsinos, one can in principle have $m_{\tilde{\ell}} > M_{\tilde{\Delta}^{--}}$ and in such a scenario the only allowed decay mode would be the 3-body decays for the doubly charged higgsinos, which would dominantly be through off-shell sleptons: $\tilde{\Delta}^{--} \rightarrow \tilde{\ell}^{*-} \ell^- \rightarrow \ell^- \ell^- \tilde{\chi}_1^0$. We focus our analysis on the final states: two like signed leptons in association with large missing energy coming from the LSP ($\tilde{\chi}_1^0$).

3.1.3 Analysis of the final states

In the rest of the analysis of final states, we will consider the 2-body and 3-body decay modes of the doubly charged higgsino ($\tilde{\Delta}_L^{--}$), and look at the resulting signal events against the most dominant SM background. We present our results for both the sample points given in Table 1 with point **A** used for a machine with $\sqrt{s} = 500$ GeV and point **B** considered for $\sqrt{s} = 1$ TeV option. In the case of *sample point A*, the mass of the doubly charged higgsino ($\tilde{\Delta}_L^{--}$) is taken to be 300 GeV and the LSP mass is 91.8 GeV, while the other neutralino states are heavy and not accessible to the decay of the doubly charged higgsino or sleptons (directly). This also makes both the 2-body $\tilde{\Delta}^{--} \longrightarrow \tilde{\ell}^- \ell^-$ and 3-body decay of $\tilde{\Delta}^{--} \rightarrow \ell^- \ell^- \tilde{\chi}_1^0$ the only allowed channels of decay. However, we point out that if the other decay modes ($\tilde{\chi}_i^0 \ell^-$, $i > 2$ and $\tilde{\chi}_i^\pm \nu_\ell$) were accessible as the decay channels of sleptons, then the only visible effect on our signal would be to reduce the branching fractions and hence decrease the signal events for our final states. But they will not change the characteristic kinematic features of the final states in consideration. In our analysis we focus on the following leptonic final states:

$$(i) \quad e^- e^- \cancel{E}, \quad (ii) \quad \mu^- \mu^- \cancel{E}$$

It is worth pointing out that the analysis for a final state $\tau^- \tau^- \cancel{E}$ will be exactly similar to $\mu^- \mu^- \cancel{E}$, provided that the ΔL couplings are identical and that we assume similar detection efficiencies for the τ 's in the final state. Thus we do not discuss the final states with τ 's

in our analysis any further. Assuming, as before, beam polarization of (-1,-1) throughout the analysis for the $\tilde{\Delta}_L^{--}$ production, the major SM background that contributes to the final states in (i) is the scattering process:

$$e^- + e^- \rightarrow e^- + e^- + \bar{\nu}_l \nu_l$$

which, although a continuum background, could *prima facie* be very large. Thus, the event

		$\sqrt{s} = 500 \text{ GeV}$		
Cuts Used		SM	signal-1	signal-2
$E_e > 5 \text{ GeV}$	$ \eta_e < 3.0$	(-, -) 537.7 fb	(-, -) 123.8 fb	(-, -) 19.9 fb
$\cancel{E} > 10 \text{ GeV}$	$\Delta R_{ee} > 0.2$	(+, +) 15.1 fb	(+, +) 486.8 fb	(+, +) 78.1 fb
$E_e > 5 \text{ GeV}$	$ \eta_e < 1.5$	(-, -) 218.0 fb	(-, -) 102.7 fb	(-, -) 16.5 fb
$\cancel{E} > 100 \text{ GeV}$	$\Delta R_{ee} > 0.2$	(+, +) 3.8 fb	(+, +) 403.98 fb	(+, +) 65.1 fb
$E_e > 5 \text{ GeV}$	$ \eta_e < 3.0$	(-, -) 280.1 fb	(-, -) 123.8 fb	(-, -) 19.9 fb
$\cancel{E} > \sqrt{s}/2 \text{ GeV}$	$\Delta R_{ee} > 0.2$	(+, +) 3.3 fb	(+, +) 468.8 fb	(+, +) 78.1 fb
$E_e > 5 \text{ GeV}$	$ \eta_e < 1.5$	(-, -) 103.8 fb	(-, -) 102.7 fb	(-, -) 16.5 fb
$\cancel{E} > \sqrt{s}/2 \text{ GeV}$	$\Delta R_{ee} > 0.2$	(+, +) 0.103 fb	(+, +) 403.98 fb	(+, +) 65.1 fb
		$\sqrt{s} = 1 \text{ TeV}$		
$E_e > 5 \text{ GeV}$	$ \eta_e < 3.0$	(-, -) 1.13 pb	(-, -) 40.5 fb	(-, -) 14.0 fb
$\cancel{E} > 10 \text{ GeV}$	$\Delta R_{ee} > 0.2$	(+, +) 12.6 fb	(+, +) 156.4 fb	(+, +) 53.9 fb
$E_e > 5 \text{ GeV}$	$ \eta_e < 1.5$	(-, -) 238.9 fb	(-, -) 33.4 fb	(-, -) 11.7 fb
$\cancel{E} > 100 \text{ GeV}$	$\Delta R_{ee} > 0.2$	(+, +) 3.1 fb	(+, +) 129.2 fb	(+, +) 45.0 fb
$E_e > 5 \text{ GeV}$	$ \eta_e < 3.0$	(-, -) 605.9 fb	(-, -) 40.5 fb	(-, -) 14.0 fb
$\cancel{E} > \sqrt{s}/2 \text{ GeV}$	$\Delta R_{ee} > 0.2$	(+, +) 0.4 fb	(+, +) 156.4 fb	(+, +) 53.9 fb
$E_e > 5 \text{ GeV}$	$ \eta_e < 1.5$	(-, -) 106.0 fb	(-, -) 33.4 fb	(-, -) 11.7 fb
$\cancel{E} > \sqrt{s}/2 \text{ GeV}$	$\Delta R_{ee} > 0.2$	(+, +) 0.007 fb	(+, +) 129.2 fb	(+, +) 45.0 fb

Table 2: Signal and SM cross sections for the $e^-e^- \cancel{E}$ final states with different choice of kinematic cuts for both signal and background at the e^-e^- collider with center-of-mass energies $\sqrt{s} = 500 \text{ GeV}$ and $\sqrt{s} = 1 \text{ TeV}$. We also show the beam polarizations in parentheses. The ΔR is defined as $(\Delta R)^2 \equiv (\Delta\phi)^2 + (\Delta\eta)^2$ with $\Delta\eta$ and $\Delta\phi$ respectively denoting the separation in rapidity and azimuthal angle for the pair of particles under consideration.

selection criteria are largely aimed at suppressing this continuum background. The SM

background for signal (ii) comes from a six-body final state

$$e^- + e^- \rightarrow \mu^- + \mu^- + \bar{\nu}_\mu \bar{\nu}_\mu + \nu_e \nu_e$$

and is quite small.

To highlight the effect of kinematic cuts in suppressing the background, we present some results in Table 2. The SM background has been calculated using the event generation package of Madgraph and Madevent [22], with slight modifications to extract the polarized cross sections. We have chosen the $|\Delta L| = 2$ coupling strength as $\tilde{f}_{ee} = 0.3$ throughout the analysis and the branching ratios for the 2-body and 3-body decays as:

$$\begin{aligned} BR(\tilde{\Delta}_L^- \rightarrow \tilde{\ell}_{iL}^- \ell_i^-) &= \frac{1}{3}, & i = e, \mu, \tau, & \quad m_{\tilde{\ell}_{iL}} < M_{\tilde{\Delta}_L^-} \\ BR(\tilde{\ell}_{iL}^- \rightarrow \ell_i^- \tilde{\chi}_1^0) &= 1, & i = e, \mu, \tau & \\ BR(\tilde{\Delta}_L^- \rightarrow \ell_i^- \ell_i^- \tilde{\chi}_1^0) &= \frac{1}{3}, & i = e, \mu, \tau, & \quad m_{\tilde{\ell}_{iL}} > M_{\tilde{\Delta}_L^-} \end{aligned}$$

where only the 3-body decay is allowed when $m_{\tilde{\ell}_{iL}} > M_{\tilde{\Delta}_L^-}$. To define our notations, we write *signal-1* to correspond to the 2-body decay of $\tilde{\Delta}_L^-$ and write *signal-2* to correspond to the 3-body decay of $\tilde{\Delta}_L^-$. We use *sample point A* for the machine with $\sqrt{s} = 500$ GeV as its center-of-mass energy and *sample point B* for the $\sqrt{s} = 1$ TeV option. We choose $M_{\tilde{\Delta}_L^-} = 300$ GeV and $m_{\tilde{\ell}_{iL}} = 150$ GeV for *signal-1*, while for *signal-2*, $m_{\tilde{\ell}_{iL}} = 400$ GeV to study the signal at the $\sqrt{s} = 500$ GeV machine. The corresponding choice for the analysis at the $\sqrt{s} = 1$ TeV option is $M_{\tilde{\Delta}_L^-} = 500$ GeV, $m_{\tilde{\ell}_{iL}} = 250$ GeV for *signal-1*, while for *signal-2*, $m_{\tilde{\ell}_{iL}} = 550$ GeV.

The background for the signal (ii) $\mu^- \mu^- \cancel{E}$ is a six-body final state and would be very small. The cuts, which gave the SM background $\sigma(e^- e^- \cancel{E}) = 537.7$ fb/1.13 pb, give cross sections: $\sigma(\mu^- \mu^- \cancel{E}) \sim \mathcal{O}(10^{-1})/\mathcal{O}(1)$ fb for, respectively, the $\sqrt{s} = 500/1000$ GeV machine. However the effect of cuts are not severe for the $\mu^- \mu^- \cancel{E}$ final states as compared to $e^- e^- \cancel{E}$ final states, where the cross section is reduced by more than $\sim 80 - 90\%$ of the original one, while the cross section in this case reduces by about 30% for the more stringent cuts listed in Table 2. Hence we have chosen to use the same set of cuts for both final states.

We present our results for the set of cuts which reduces the background while keeping the signal relatively large. Our choice of cuts for the signal-background analysis is as follows:

- We demand that the electrons respect a minimum rapidity cut of $|\eta_e| < 1.5$ which is the most effective cut to reduce the large continuum background. The signal is peaked

at $\eta_e = 0$, while the SM background is peaked for $|\eta_e| > 1.5$, which is predominantly due to the strong t-channel photon contribution in the $e^-e^- \cancel{E}$ final states.

- The final state electrons must carry a minimum energy, $E_e > 5$ GeV.
- We also demand a large cut on the missing energy because of the massive LSP in the final state for the signal, $\cancel{E} > \sqrt{s}/2$ GeV.
- To ensure proper resolution between the final state electrons we demand that they are well separated in space and satisfy $\Delta R_{ee} > 0.2$.

Using the above cuts, we can see from Table 2 that the large SM background which previously overwhelmed the signal for the most conservative cuts, is effectively suppressed without losing out much on the signal events.

We present the different kinematic distributions in figures 5, 6, 7, 8 and 9 for the final

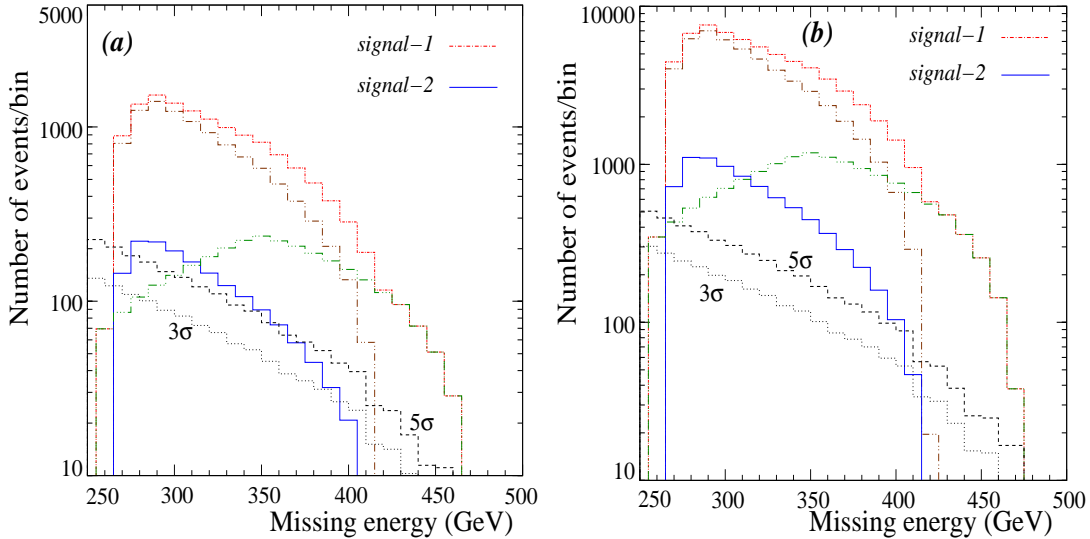


Figure 5: Binwise distribution of missing energy for both *signal-1* and *signal-2* for the final states $e^-e^- \cancel{E}$ ($\sqrt{s} = 500$ GeV). The broken ($-\cdots-$) brown lines correspond to the signal through $\tilde{\Delta}_L^{--}$ production while the broken ($-\cdots-$) green lines correspond to the signal events from \tilde{e}_L^{--} -pair production. Also shown in dashed and dotted dark lines are the 5σ and 3σ fluctuations in the SM background. Each binsize is 10 GeV. (a) $\mathcal{L} = 100 fb^{-1}$, (b) $\mathcal{L} = 500 fb^{-1}$.

states $e^-e^- \cancel{E}$ for the 500 GeV machine. We must point out that the SM background for the other final state $\mu^-\mu^- \cancel{E}$ at the 500 GeV machine turns out to be completely insignificant and

the signal would be background free. In fact the signal would also act as an obvious hint for scenarios with doubly charged higgsinos and provide strong distinguishing features from the typical MSSM signal coming from selectron pair production ($e^-e^- \rightarrow \tilde{e}_L^- \tilde{e}_L^-$), which produces an identical final state $e^-e^- \cancel{E}$ but gives no contribution to the $\mu^- \mu^- \cancel{E}$ final states. Having said this, we must note that for the $e^-e^- \cancel{E}$ final states, we have additional events coming from $e^-e^- \rightarrow \tilde{e}_L^- \tilde{e}_L^-$ in this model too. Looking at our mass spectrum, this production mode will only contribute to *signal-1*. We estimate this to be 29.72 fb at the 500 GeV machine for the polarization choice (-1,-1) and the same set of cuts. We include this contribution in *signal-1* for all the figures (5–9), and the integrated luminosity taken in (a) and (b) is 100 and 500 fb^{-1} respectively. We have also shown the independent contributions for *signal-1* coming from $\tilde{\Delta}_L^{--}$ and \tilde{e}_L^- -pair production in Figs. 5, 6 and 9 to highlight the difference in the two cases. As mentioned earlier, the doubly charged higgsino mass is taken to be 300 GeV, while the selectron masses are 150 GeV and 400 GeV for *signal-1* and *signal-2* respectively.

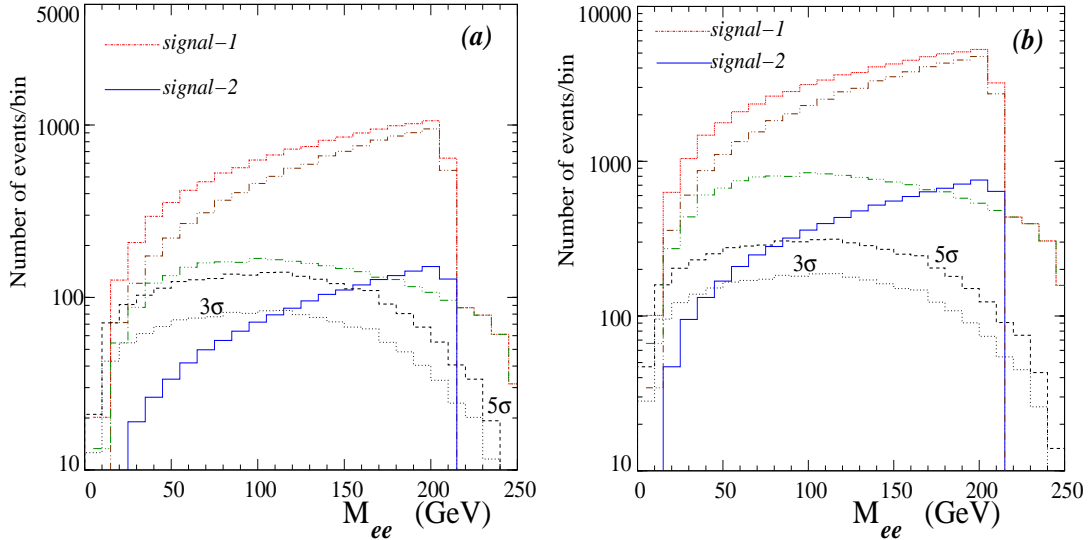


Figure 6: Binwise distribution of the invariant mass of the visible particles in the final state $e^-e^- \cancel{E}$ for both *signal-1* and *signal-2* ($\sqrt{s} = 500 \text{ GeV}$). The broken ($-\cdots-$) brown lines correspond to the signal through $\tilde{\Delta}_L^{--}$ production while the broken ($-\cdots-$) green lines correspond to the signal events from \tilde{e}_L^- -pair production. The background follows the notation of Fig 5. Each binsize is 10 GeV. (a) $\mathcal{L} = 100 \text{ fb}^{-1}$, (b) $\mathcal{L} = 500 \text{ fb}^{-1}$.

In Fig. 5 we plot the binwise distribution of missing energy for both *signal-1* and *signal-2*, represented by colored histograms, and compare it with the expected statistical (Gaussian)

fluctuations at the 3 and 5 standard deviations of the SM background. As expected, the signal would be associated with a large missing energy due to the presence of LSP in the final state, and this also allows to set a strong cut on the missing energy. In Fig. 5(a) we show the distribution for an integrated luminosity of 100 fb^{-1} and find that *signal-1* stands out quite distinctly against a 5σ fluctuation in the SM background. The fact that the signal is actually superimposed over the tail end of the much wider missing energy distribution of the SM, carried by the neutrinos, makes *signal-1* stand out against such large fluctuations in the SM background. We show the same distribution in Fig. 5(b) with an integrated luminosity of 500 fb^{-1} , where both *signal-1* and *signal-2* stand out against a 5σ fluctuations in the background.

In Fig. 6 we show the invariant mass distribution for the pair of visible particles in the final state. As both the visible leptons come from the (cascade) decay of $\tilde{\Delta}_L^{--}$, the distribution for the signal would depend strongly on the masses of $\tilde{\Delta}_L^{--}$ and $\tilde{\chi}_1^0$'s in the final state, and the distribution exhibits a sharp kinematic edge which highlights this dependence. The location of this kinematic edge can be well approximated by the formula

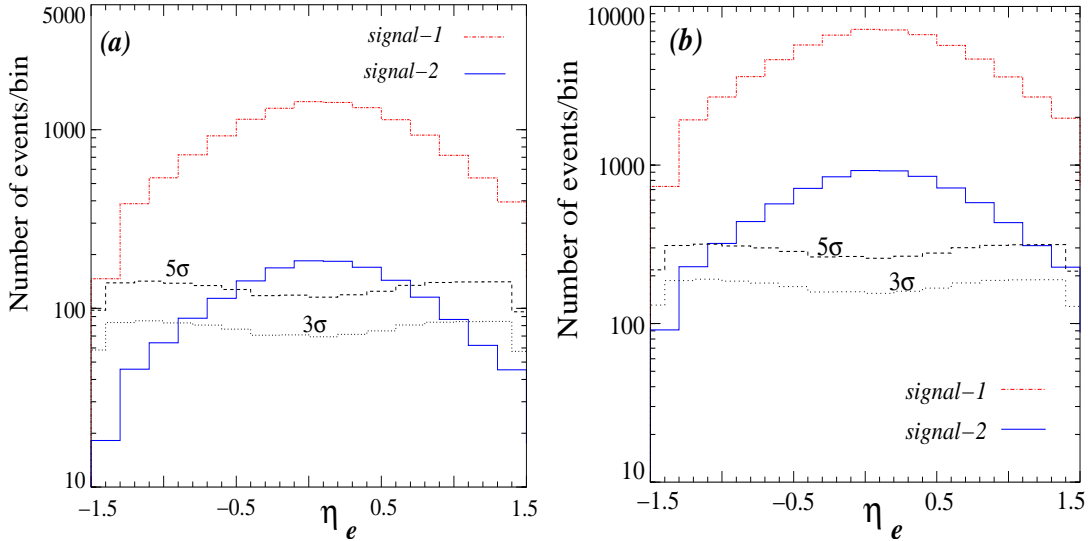


Figure 7: Binwise distribution of the rapidity of the e^- in the final state $e^- e^- \cancel{E}$ for both *signal-1* and *signal-2* ($\sqrt{s} = 1 \text{ TeV}$). The background follows the notation of Fig 5. Each binsize is 0.2 radians. (a) $\mathcal{L} = 100 \text{ fb}^{-1}$, (b) $\mathcal{L} = 500 \text{ fb}^{-1}$.

$$M_{ee}^{edge} \approx \sqrt{M_{\tilde{\Delta}_L^{--}}^2 + M_{\tilde{\chi}_1^0}^2 - \sqrt{s} M_{\tilde{\chi}_1^0}}$$

where we have assumed that the final neutralino coming from the cascade decay of $\tilde{\Delta}_L^{--}$ carries a negligible 3-momentum, as its mass is nearly a third of the mass of $\tilde{\Delta}_L^{--}$. This is in sharp contrast to the SM distribution, where the background has a more uniform invariant mass distribution. In fact, the distribution arising from the independent contribution of \tilde{e}_L -pair production shown in broken ($-\cdots-$) green line has a uniform distribution like the SM background, but is overwhelmed by the events coming from the $\tilde{\Delta}_L^{--}$ production. The luminosity choices are as for the plots in Fig. 6(a) and (b).

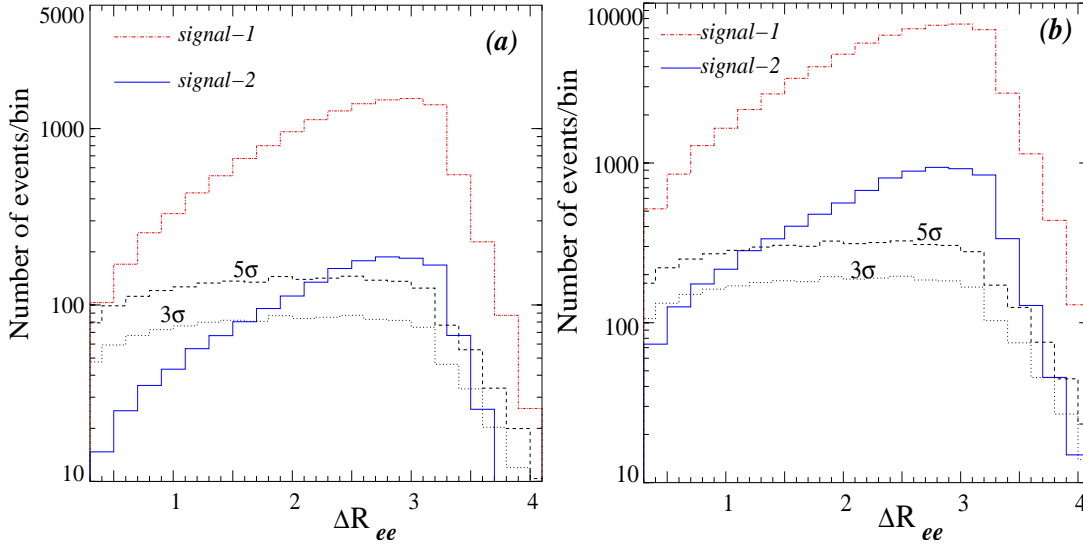


Figure 8: Binwise distribution of the ΔR between the visible particles in the final state $e^-e^-\cancel{E}$ for both *signal-1* and *signal-2* ($\sqrt{s} = 500 \text{ GeV}$). The background follows the notation of Fig 5. Each binsize is 0.2. (a) $\mathcal{L} = 100 \text{ fb}^{-1}$, (b) $\mathcal{L} = 500 \text{ fb}^{-1}$.

In Fig. 7 and Fig. 8, we give the rapidity distribution for the final state leptons and the ΔR distribution between the pair of visible particles in the final state respectively. The rapidity distribution clearly suggests that the leptons in the signal distribution emerge back to back, since the distribution peaks at $\eta = 0$. This is because the leptons are decay products of a massive $\tilde{\Delta}^{--}$ which has low boost, and hence it is more likely to give off back to back lepton-slepton in *signal-1*, while the other lepton coming from the heavy slepton is most likely to carry the maximum boost of the slepton as it is produced against a massive particle ($\tilde{\chi}_1^0$) with less boost. The distribution for *signal-2* shows a similar behavior because the 2-lepton system recoils against a massive LSP which would have a minimum boost. For the background, the distribution is mostly peaked at large values of $|\eta|$ due to the strong

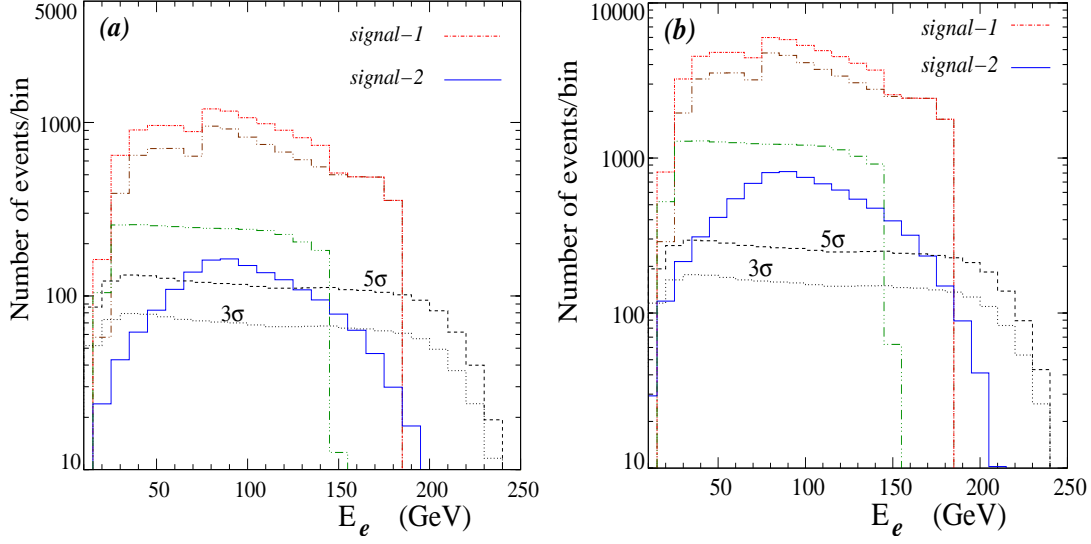


Figure 9: Binwise distribution of the energy of e^- in the final state $e^-e^-\cancel{E}$ for both *signal-1* and *signal-2* ($\sqrt{s} = 500$ GeV). The broken ($-\cdots-$) brown lines correspond to the signal through $\tilde{\Delta}_L^{--}$ production while the broken ($-\cdots-$) green lines correspond to the signal events from \tilde{e}_L^- -pair production. The background follows the notation of Fig 5. Each binsize is 10 GeV. (a) $\mathcal{L} = 100 fb^{-1}$, (b) $\mathcal{L} = 500 fb^{-1}$.

t -channel contribution from the photon exchange, as discussed earlier. This actually helps suppress the huge continuum background in the case of $e^-e^-\cancel{E}$ final states, as shown in Table 2. The distribution in ΔR_{ee} also shows a clear difference in behavior from the SM background, which can again be attributed to the fact that the angular distributions for the final state charged leptons in the signal events are markedly different from those of the SM events, and if one considers

$$|\Delta\eta| = |\eta_{e^-}^1 - \eta_{e^-}^2|$$

the distribution actually shows a peak for the signal at $|\Delta\eta| = 0$, while for the SM background the signal peaks beyond $|\Delta\eta| > 1.2$.

Finally we present the energy distribution of the charged leptons for the two different final states in Fig. 9. The signal is again seen to stand out against the 5σ fluctuations in the SM background for both *signal-1* and *signal-2* for the higher integrated luminosity of $500 fb^{-1}$ in Fig. 9(b). The more interesting feature is seen for *signal-1*, where the energy distributions for the final two charged leptons will in principle be different. Assuming that it would be difficult to distinguish between the two leptons, we show the distribution by

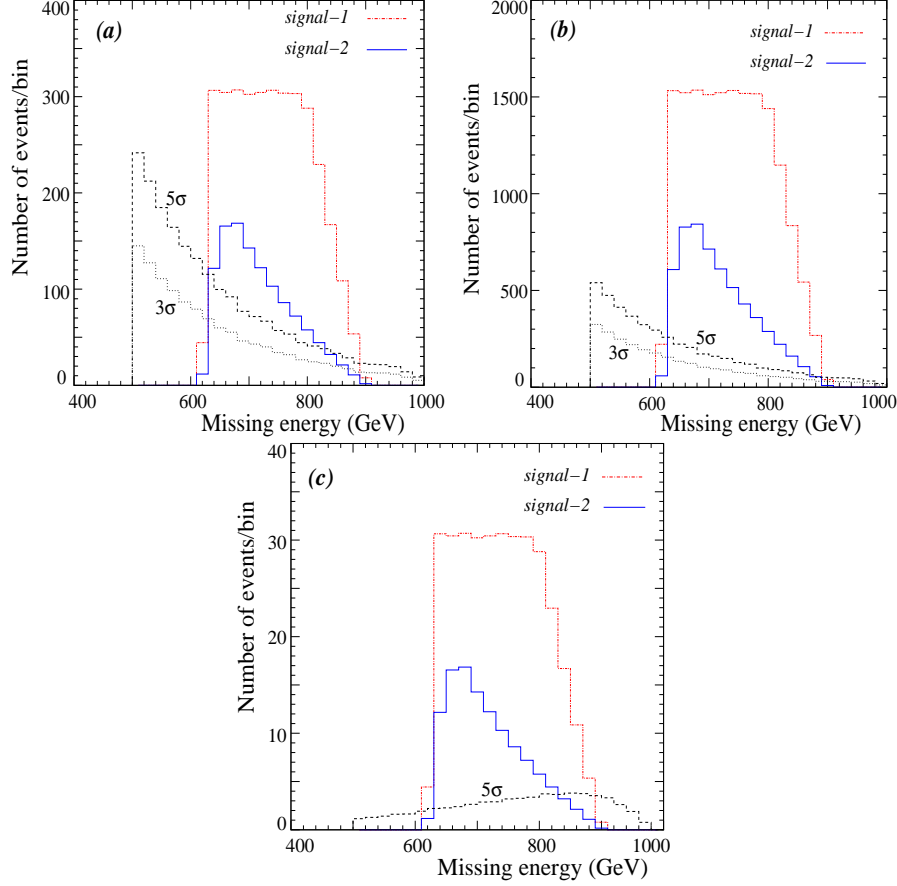


Figure 10: Binwise distribution of missing energy for both *signal-1* and *signal-2* ($\sqrt{s} = 1$ TeV). The background follows the notation of Fig 5. Each binsize is 20 GeV. (a) $\mathcal{L} = 100fb^{-1}$ (final state $e^-e^-\cancel{E}$), (b) $\mathcal{L} = 500fb^{-1}$ (final state $e^-e^-\cancel{E}$), (c) $\mathcal{L} = 10fb^{-1}$ (final state $\mu^-\mu^-\cancel{E}$). Here $M_{\tilde{\Delta}_L^{--}} = 500$ GeV. For *signal-1* $m_{\tilde{e}_L} = 250$ GeV and for *signal-2* $m_{\tilde{e}_L} = 500$ GeV.

taking the average of both the leptons energy distributions. However, in the case of *signal-1* the leptons coming from the 2-body decay of slepton will have an energy profile depending on the mass difference $m_{\tilde{\ell}} - M_{\tilde{\chi}_1^0}$, while the lepton which comes from the 2-body decay of $\tilde{\Delta}^{--}$ will have an energy profile dominantly depending on $M_{\tilde{\Delta}^{--}} - m_{\tilde{\ell}}$. For *signal-2* however, both leptons have identical distributions which depend on the 3-body decay kinematics of the parent particle.

In Figs. 10, 11 and 12 we show the distributions for the total missing energy, invariant mass of the visible leptons and the energy profile of the final state leptons for the machine with $\sqrt{s} = 1$ TeV center-of-mass energy for the *sample point B* given in Table 1. The mass for $\tilde{\Delta}_L^{--}$ is taken as 500 GeV while the corresponding masses of the selectrons for *signal-1* and

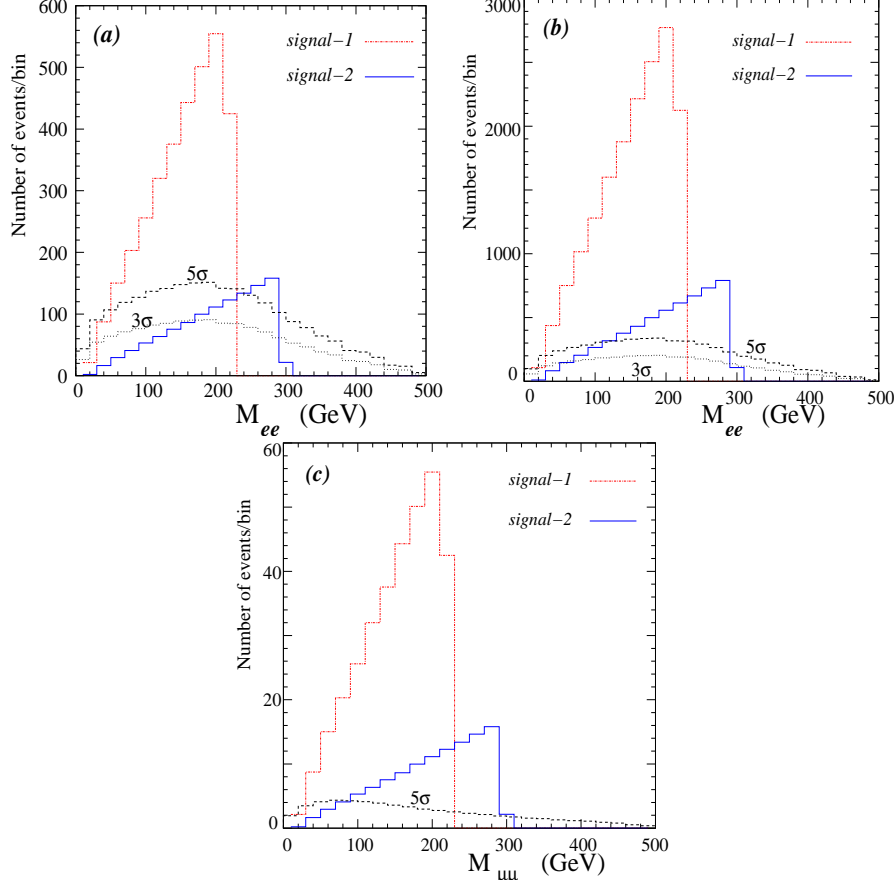


Figure 11: Binwise distribution of the invariant mass of the visible particles in the final state for both *signal-1* and *signal-2*. Each binsize is 20 GeV ($\sqrt{s} = 1$ TeV). The background follows the notation of Fig 5. (a) $\mathcal{L} = 100 fb^{-1}$ (final state $e^-e^-\cancel{E}$), (b) $\mathcal{L} = 500 fb^{-1}$ (final state $e^-e^-\cancel{E}$), (c) $\mathcal{L} = 10 fb^{-1}$ (final state $\mu^-\mu^-\cancel{E}$). Here $\sqrt{s} = 1$ TeV and $M_{\tilde{\Delta}_L^{--}} = 500$ GeV. For *signal-1* $m_{\tilde{e}_L} = 250$ GeV and for *signal-2* $m_{\tilde{e}_L} = 500$ GeV.

signal-2 are 250 GeV and 550 GeV respectively. The contribution to *signal-1* from \tilde{e}_L^- -pair production in this case is however very small ($0.2 fb$) and does not have any significant effect on the distributions. In each of the plots we also show the distributions for the final states $\mu^-\mu^-\cancel{E}$. Here, in addition to distributions given for integrated luminosities $\mathcal{L} = 100 fb^{-1}$ and $\mathcal{L} = 500 fb^{-1}$, we also include the case (c) $\mathcal{L} = 10 fb^{-1}$. The signal is quite large for heavier $\tilde{\Delta}_L^{--}$ and the signal far overwhelms the background for the $\mu^-\mu^-\cancel{E}$. It can be seen in all the Figs. 10, 11 and 12 that we still have a large SM background and that an integrated luminosity of $\mathcal{L} = 500 fb^{-1}$ is needed for a significant 5σ -signal for *signal-2* for the $e^-e^-\cancel{E}$ final state. The SM background for the $\mu^-\mu^-\cancel{E}$ final state is however still quite suppressed

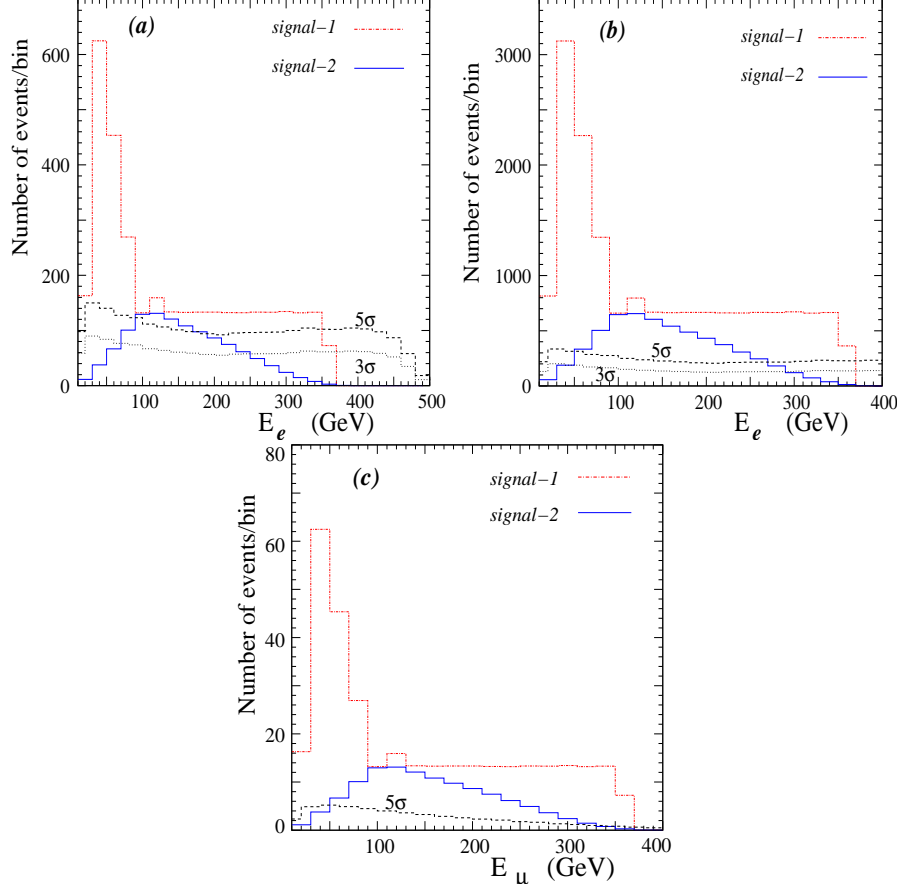


Figure 12: Binwise distribution of the energy of $e^-(\mu^-)$. The background follows the notation of Fig 5. Each binsize is 20 GeV ($\sqrt{s} = 1$ TeV). (a) $\mathcal{L} = 100fb^{-1}$ (final state $e^-e^-\cancel{E}$), (b) $\mathcal{L} = 500fb^{-1}$ (final state $e^-e^-\cancel{E}$), (c) $\mathcal{L} = 10fb^{-1}$ (final state $\mu^-\mu^-\cancel{E}$). Here $\sqrt{s} = 1$ TeV and $M_{\tilde{\Delta}_L^{--}} = 500$ GeV. For *signal-1* $m_{\tilde{e}_L} = 250$ GeV and for *signal-2* $m_{\tilde{e}_L} = 500$ GeV.

and one can observe the large rates for both *signal-1* and *signal-2* as compared to the 5σ statistical fluctuations in the SM for $\mathcal{L} = 10fb^{-1}$. We preferred to show the distributions on a linear scale as opposed to the earlier plots, since the rates for both *signal-1* and *signal-2* do not differ by a large factor. The distributions do not exhibit any additional new features as compared to the plots for the same kinematic variables at the $\sqrt{s} = 500$ GeV machine. However a look at Table 2 suggests that a heavier $\tilde{\Delta}^{--}$ accessible at a $\sqrt{s} = 1$ TeV machine will have a substantial SM background and the signal-background analysis merits discussion.

3.2 The right-handed higgsino $\tilde{\Delta}_R^{--}$

We briefly discuss the production and decay of the right chiral higgsino $\tilde{\Delta}_R^{--}$ at the e^-e^-

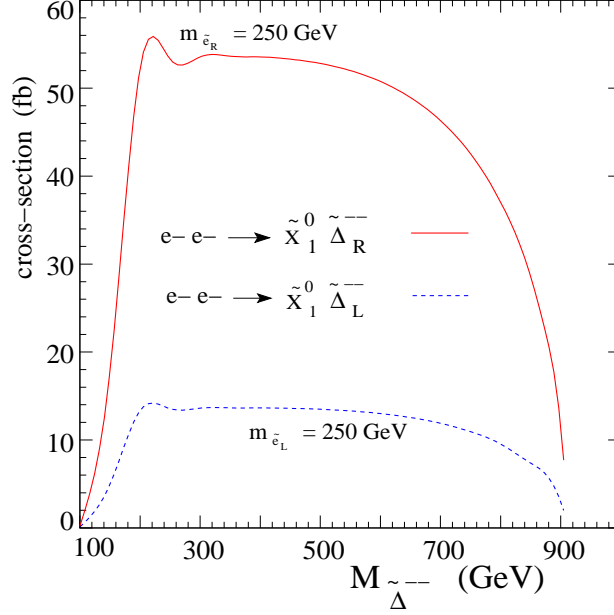


Figure 13: The production cross section as a function of the triplet higgsino mass ($\sqrt{s} = 1$ TeV). The cross section for both $\tilde{\Delta}_L^{--}$ and $\tilde{\Delta}_R^{--}$. The solid (red) line corresponds to $\tilde{\Delta}_R^{--}$ production with the beam polarizations $(+1, +1)$ while the broken (blue) line corresponds to $\tilde{\Delta}_L^{--}$ production with the beam polarizations $(-1, -1)$. The plots shown are for the sample point **A** given in Table 1.

collider, emphasizing distinguishing features with respect to $\tilde{\Delta}_L^{--}$. In Fig. 13 we show the production cross section for its production and compare it with the production cross section of $\tilde{\Delta}_L^{--}$. Note that the production of the right-chiral $\tilde{\Delta}_R^{--}$ requires the electron beams to be dominantly right-polarized and can be quite large compared to the production cross section of the $\tilde{\Delta}_L^{--}$, as shown in Fig. 13. The difference is mainly due to the difference in coupling of the neutralino with $e - \tilde{e}_{L(R)}$ which in this case reads,

$$\ell^- \tilde{\ell}_R \chi_k^0 \rightarrow \frac{1}{\sqrt{2}} (g_R N_{k2}^* + g_V N_{k3}^*) P_R$$

The production of the right-chiral $\tilde{\Delta}_R^{--}$ will have a very clean signal as the SM background is completely reducible using polarization of the beams. We have already listed the SM background in Table 2 corresponding to different beam polarizations. The right-polarized beams effectively kill the SM background because the dominant contributions come from W-boson exchange which vanish when the electron beams are right-polarized. So the signal for the $\tilde{\Delta}_R^{--}$ production is relatively background free. In fact, this suggests that the signals for the right-handed $\tilde{\Delta}_R^{--}$ will be even more striking and hence much lower values of the

$\Delta L = 2$ couplings can be probed. To highlight this fact and to illustrate the sensitivity of the signal to the ΔL coupling, we calculate the rates for different values of the ΔL coupling \tilde{f}_{ee} . We plot the distributions in the missing energy, invariant mass of the visible leptons and the energy of the visible lepton in the final state for the $e^-e^- \cancel{E}$ final state, coming from the \tilde{e}_R^- -pair production and $\tilde{\Delta}_R^-$ production, and the subsequent decays in Fig 14, for three

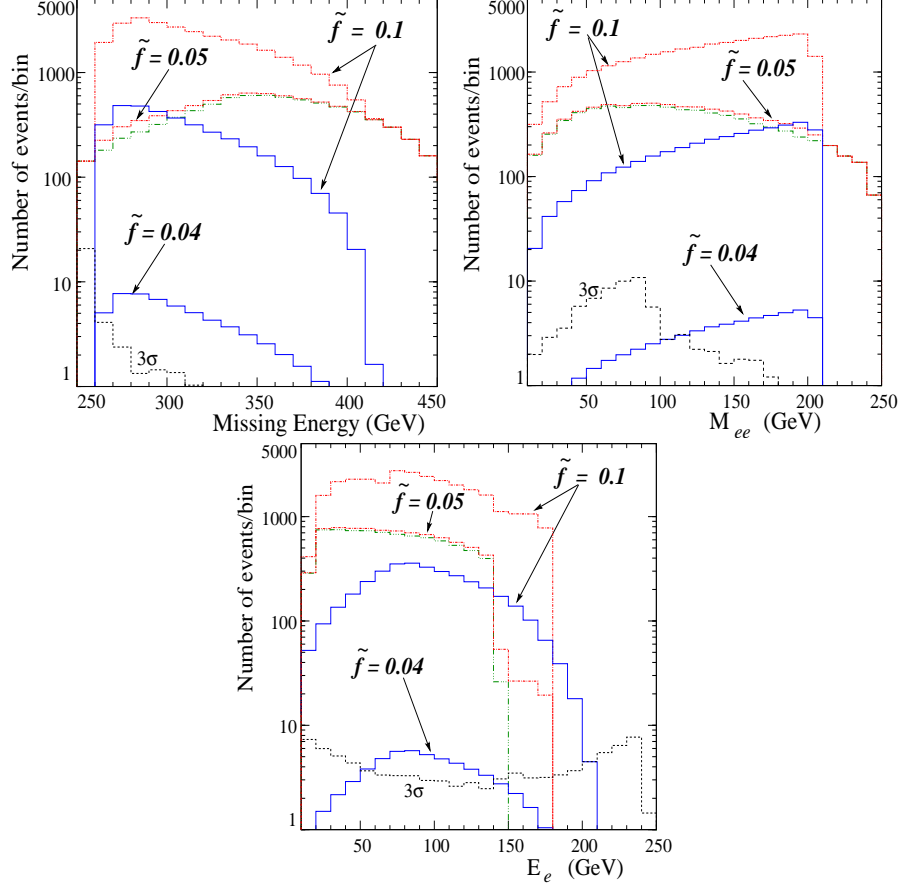


Figure 14: Binwise distribution of missing energy, invariant mass and energy of e^- for different values of the $\Delta L = 2$ coupling \tilde{f}_{ee} . The statistical fluctuations in the SM background is shown at 3σ in black (dashed) lines. Each binsize is 10 GeV while the luminosity is taken as $\mathcal{L} = 500 fb^{-1}$ (final state $e^-e^- \cancel{E}$). The green ($-\cdot-\cdot-$) line stands for the independent contribution from \tilde{e}_R^- -pair production for *signal-1*. Here $\sqrt{s} = 500$ GeV and $M_{\tilde{\Delta}_R^-} = 300$ GeV. For *signal-1* shown in red lines, $m_{\tilde{e}_R} = 150$ GeV and for *signal-2* shown in blue lines, $m_{\tilde{e}_R} = 400$ GeV.

values of $\tilde{f}_{ee} = 0.04, 0.05$ and 0.1 . We consider a luminosity of $\mathcal{L} = 500 fb^{-1}$ and show the 3σ fluctuations in the SM background. All the figures clearly show that *signal-1* stands out against the background for a ΔL coupling strength which can be as low as $\tilde{f}_{ee} = 0.05$ and

even lower values can be accessed if we have $\mu^-\mu^- \not{E}$ final states. The green $(-\cdots-)$ line stands for the independent contribution coming from \tilde{e}_R^- -pair production for *signal-1*. For the polarization choice $(+1,+1)$, the cross section becomes 15.8 fb . One can see that for $\tilde{f}_{ee} \rightarrow 0$ the distribution for *signal-1* will converge on the green $(-\cdots-)$ line as the contribution coming from the $\tilde{\Delta}_R^{--}$ production becomes negligibly small. The plot shown for *signal-2*, however shows the direct reach for the coupling \tilde{f}_{ee} as the selectron-pair production is kinematically disfavored for a right-selectron mass of 400 GeV.

4 Summary and Conclusions

The absence of $\Delta L = 2$ processes in the SM provides an unique platform to search for beyond the SM scenarios. Such processes arise naturally at an e^-e^- collider where they can be produced directly. LRSUSY models where R-parity is conserved, give rise to such doubly charged exotics which can be relatively light and accessible at future linear accelerators. In this work, we have studied in detail the production of a single doubly charged higgsino and its decay channels at the ILC operating in the e^-e^- mode. We showed that the production cross sections for the $\tilde{\Delta}^{--}$ can be quite large if the beams are polarized and that enough statistics is available to study the signals arising from its subsequent decays against the dominant SM background. We have also shown how kinematic cuts can effectively limit this background and give a clear signal for LRSUSY at an e^-e^- collider. We described how different final states ($e^-e^- \not{E}$, $\mu^-\mu^- \not{E}$) compare against the dominant SM background. The use of polarized beams helps in producing doubly charged higgsinos of different chirality and hence proves to be an essential tool in distinguishing between the two chiral states of the $\tilde{\Delta}^{--}$ producing the same final states. We also find that the production of the right chiral higgsino $\tilde{\Delta}_R^{--}$ can be relatively background free and is more sensitive to lower values of the $\Delta L = 2$ coupling. This is a major advantage over the production of these exotics at hadron colliders or in e^+e^- collisions where ascertaining the chiral nature of $\tilde{\Delta}^{--}$ will be a non-trivial issue. A dominantly right (left)-polarized option for both the electron beams can achieve this quite easily at the e^-e^- collider. As most studies of LRSUSY expect the doubly-charged higgsinos to be light, and even allow for the next to lightest supersymmetric particle (NLSP) to be the right-handed doubly charged higgsino [9], the resulting signals could be spectacular.

To summarize, in this work we have shown that an e^-e^- collider can be an ideal machine to study the production of doubly charged higgsinos of the LRSUSY model. Through the choice of a few representative points in the parameter space of the model, we have shown signals coming from the production of $\tilde{\Delta}^{--}$ for two center-of-mass energies $\sqrt{s} = 500$ GeV and $\sqrt{s} = 1$ TeV. We have shown that through the final states $\ell^-\ell^-\cancel{E}$ we have clear signals for these exotics. We also find that when $\ell = \mu, \tau$ the SM background is a six-body final state and hugely suppressed. We have also highlighted the advantage of using polarized beams in producing these exotics and suppressing the SM background.

Acknowledgments

The authors would like to thank F. Maltoni for useful technical guidance regarding the use of Madgraph. The work of MF was funded by NSERC of Canada under the grant number 0105354. KH and SKR greatly acknowledge support from the Academy of Finland (project number 115032).

5 Appendix

In what follows, we use the conventions of [23].

5.1 Charginos

In the supersymmetric sector of the model there are four doubly charged higgsinos $\tilde{\Delta}_L^{--}, \tilde{\delta}_L^{++}, \tilde{\Delta}_R^{--}$, and $\tilde{\delta}_R^{++}$. The mass terms relevant to these higgsinos are:

$$\mathcal{L}_{\tilde{\Delta}} = -M_{\tilde{\Delta}^{--}}\tilde{\Delta}_L^{--}\tilde{\delta}_L^{++} - M_{\tilde{\Delta}^{--}}\tilde{\Delta}_R^{--}\tilde{\delta}_R^{++} + h.c., \quad (6)$$

where in our notation $M_{\tilde{\Delta}^{--}} = \mu_3$. The model also has six singly-charged charginos, corresponding to $\tilde{\lambda}_L, \tilde{\lambda}_R, \tilde{\phi}_u, \tilde{\phi}_d, \tilde{\Delta}_L^{\pm}$, and $\tilde{\Delta}_R^{\pm}$.

The terms relevant to the masses of charginos in the Lagrangian are

$$\mathcal{L}_C = -\frac{1}{2}(\psi^{+T}, \psi^{-T}) \begin{pmatrix} 0 & X^T \\ X & 0 \end{pmatrix} \begin{pmatrix} \psi^+ \\ \psi^- \end{pmatrix} + \text{H.c.} , \quad (7)$$

where $\psi^{+T} = (-i\lambda_L^+, -i\lambda_R^+, \tilde{\phi}_{1d}^+, \tilde{\phi}_{1u}^+, \tilde{\Delta}_L^+, \tilde{\Delta}_R^+)$ and $\psi^{-T} = (-i\lambda_L^-, -i\lambda_R^-, \tilde{\phi}_{2d}^-, \tilde{\phi}_{2u}^-, \tilde{\delta}_L^-, \tilde{\delta}_R^-)$, and

$$X = \begin{pmatrix} M_L & 0 & 0 & g_L \kappa_d & \sqrt{2} g_L v_{\delta_L} & 0 \\ 0 & M_R & 0 & g_R \kappa_d & 0 & \sqrt{2} g_R v_{\delta_R} \\ g_L \kappa_u & g_R \kappa_u & 0 & -\mu_1 & 0 & 0 \\ 0 & 0 & -\mu_1 & 0 & 0 & 0 \\ \sqrt{2} g_L v_{\Delta_L} & 0 & 0 & 0 & -\mu_3 & 0 \\ 0 & \sqrt{2} g_R v_{\Delta_R} & 0 & 0 & 0 & -\mu_3 \end{pmatrix}, \quad (8)$$

where we have taken, for simplification, $\mu_{ij} = \mu_1$. Here κ_u and κ_d are the bidoublet Higgs bosons vacuum expectation values (VEVs), v_{Δ_R} and v_{δ_R} are the triplet Higgs bosons VEVs, and M_L, M_R the $SU(2)_L$ and $SU(2)_R$ gaugino masses, respectively. The chargino mass eigenstates χ_i are obtained by

$$\chi_i^+ = V_{ij} \psi_j^+, \quad \chi_i^- = U_{ij} \psi_j^-, \quad i, j = 1, \dots, 5, \quad (9)$$

with V and U unitary matrices satisfying

$$U^* X V^{-1} = M_D. \quad (10)$$

The diagonalizing matrices U^* and V are obtained by computing the eigenvectors corresponding to the eigenvalues of XX^\dagger and $X^\dagger X$, respectively.

5.2 Neutralinos

The model has eleven neutralinos, corresponding to $\tilde{\lambda}_Z, \tilde{\lambda}_{Z'}, \tilde{\lambda}_{B-L}, \tilde{\phi}_{1u}^0, \tilde{\phi}_{2u}^0, \tilde{\phi}_{1d}^0, \tilde{\phi}_{2d}^0, \tilde{\Delta}_L^0, \tilde{\Delta}_R^0, \tilde{\delta}_L^0$, and $\tilde{\delta}_R^0$. The terms relevant to the masses of neutralinos in the Lagrangian are

$$\mathcal{L}_N = -\frac{1}{2} \psi^{0T} Y \psi^0 + H.c. , \quad (11)$$

where $\psi^0 = (-i\lambda_L^0, -i\lambda_R^0, -i\lambda_{B-L}, \tilde{\phi}_{1u}^0, \tilde{\phi}_{2d}^0, \tilde{\Delta}_L^0, \tilde{\delta}_L^0, \tilde{\Delta}_R^0, \tilde{\delta}_R^0)^T$. We omit $(\tilde{\phi}_{1d}^0, \tilde{\phi}_{2u}^0)^T$, which only mix with each other. The mixing matrix is:

$$Z = \begin{pmatrix} M_L & 0 & 0 & -\frac{g_L \kappa_u}{\sqrt{2}} & \frac{g_L \kappa_d}{\sqrt{2}} & -2^{\frac{1}{2}} g_L v_{\Delta_L} & -2^{\frac{1}{2}} g_L v_{\delta_L} & 0 & 0 \\ 0 & M_R & 0 & \frac{g_L \kappa_u}{\sqrt{2}} & \frac{g_L \kappa_d}{\sqrt{2}} & 0 & 0 & -2^{\frac{1}{2}} g_R v_{\Delta_R} & -2^{\frac{1}{2}} g_R v_{\delta_R} \\ 0 & 0 & M_{B-L} & 0 & 0 & 2^{\frac{3}{2}} g_V v_{\Delta_L} & 2^{\frac{3}{2}} g_V v_{\delta_L} & 2^{\frac{3}{2}} g_V v_{\Delta_R} & 2^{\frac{3}{2}} g_V v_{\delta_R} \\ -\frac{g_L \kappa_u}{\sqrt{2}} & \frac{g_R \kappa_u}{\sqrt{2}} & 0 & 0 & \mu_1 & 0 & 0 & 0 & 0 \\ \frac{g_L \kappa_d}{\sqrt{2}} & -\frac{g_R \kappa_d}{\sqrt{2}} & 0 & \mu_1 & 0 & 0 & 0 & 0 & 0 \\ -2^{\frac{1}{2}} g_L v_{\Delta_L} & 0 & 2^{\frac{3}{2}} g_V v_{\Delta_L} & 0 & 0 & 0 & -\mu_3 & 0 & 0 \\ -2^{\frac{1}{2}} g_L v_{\delta_L} & 0 & 2^{\frac{3}{2}} g_V v_{\delta_L} & 0 & 0 & -\mu_3 & 0 & 0 & 0 \\ 0 & -2^{\frac{1}{2}} g_R v_{\Delta_R} & 2^{\frac{3}{2}} g_V v_{\Delta_R} & 0 & 0 & 0 & 0 & 0 & -\mu_3 \\ 0 & -2^{\frac{1}{2}} g_R v_{\delta_R} & 2^{\frac{3}{2}} g_V v_{\delta_R} & 0 & 0 & 0 & 0 & -\mu_3 & 0 \end{pmatrix} \quad (12)$$

The mass eigenstates are defined by

$$\chi_i^0 = N_{ij} \psi_j^0 \quad (i, j = 1, 2, \dots, 9), \quad (13)$$

where N is a unitary matrix chosen such that

$$N Z N^T = Z_D, \quad (14)$$

and Z_D is a diagonal matrix with non-negative entries.

5.3 Scalars

The interactions between vector bosons and scalars arise from the kinetic energy term for the gauge bosons in the Lagrangian density. We denote by $x_{L,R}$ the Higgs fields before mixing, and by $y_{L,R}$ the Higgs fields after mixing. The Higgs scalar fields are defined as:

Doubly Charged Fields

$$\begin{aligned} x_R^{++T} &\equiv (\Delta_R^{++} \quad \delta_R^{--*}), \quad x_R^{--T} \equiv (\Delta_R^{++*} \quad \delta_R^{--}) \\ y_R^{\pm\pm T} &\equiv (H_1^{\pm\pm} \quad H_2^{\pm\pm}) \\ x_L^{++T} &\equiv (\Delta_L^{++} \quad \delta_L^{--*}), \quad x_L^{--T} \equiv (\Delta_L^{++*} \quad \delta_L^{--}) \\ y_L^{\pm\pm T} &\equiv (H_3^{\pm\pm} \quad H_4^{\pm\pm}) \end{aligned} \quad (15)$$

Singly Charged Fields

$$\begin{aligned}
x^{+T} &\equiv \left(\Delta_L^+ \ \delta_L^{-*} \ \phi_{2d}^{-*} \ \phi_{1u}^+ \ \phi_{2u}^{-*} \ \phi_{1d}^+ \ \Delta_R^+ \ \delta_R^{-*} \right), \\
x^{-T} &\equiv \left(\Delta_L^{+*} \ \delta_L^- \ \phi_{2d}^- \ \phi_{1u}^{+*} \ \phi_{2u}^- \ \phi_{1d}^{+*} \ \Delta_R^{+*} \ \delta_R^- \right), \\
y^{\pm T} &\equiv \left(H_1^\pm \ H_2^\pm \ H_3^\pm \ H_4^\pm \ H_5^\pm \ H_6^\pm \ G_1^\pm \ G_2^\pm \right)
\end{aligned} \tag{16}$$

Neutral Fields

$$\begin{aligned}
x_s^{0T} &\equiv \left(H_{\Delta_L} \ H_{\delta_L} \ H_{1d}^0 \ H_{2u}^0 \ H_{1u}^0 \ H_{2d}^0 \ H_{\Delta_R} \ H_{\delta_R} \right), \\
y_s^{0T} &\equiv \left(H_1^0 \ H_2^0 \ H_3^0 \ H_4^0 \ H_5^0 \ H_6^0 \ H_7^0 \ H_8^0 \right), \\
x_p^{0T} &\equiv \left(z_{\Delta_L} \ z_{\delta_L} \ z_{1d}^0 \ z_{2u}^0 \ z_{1u}^0 \ z_{2d}^0 \ z_{\Delta_R} \ z_{\delta_R} \right), \\
y_p^{0T} &\equiv \left(A_1^0 \ A_2^0 \ A_3^0 \ A_4^0 \ A_5^0 \ A_6^0 \ G_1^0 \ G_2^0 \right)
\end{aligned} \tag{17}$$

where the indices "s" and "p" stand for scalar and pseudoscalar, respectively. There are two charged Goldstone bosons for the left-handed and the right-handed charged vector bosons, and two neutral Goldstone bosons for the Z_L and Z_R bosons. They have zero mass. We define them to be the 7-th and 8-th component of H^\pm and A^0 , in order to simplify the summation convention. The mass matrices M are real and symmetric and diagonalized by orthogonal matrices R defines as:

$$\begin{aligned}
\left(R_R^{\pm\pm} \right)_{ij} \left(M_R^{\pm\pm} \right)_{jk} \left(R_R^{\pm\pm} \right)_{lk} &= \text{diag} \left(m_1^{\pm\pm}, m_2^{\pm\pm} \right), \\
\left(R_L^{\pm\pm} \right)_{ij} \left(M_L^{\pm\pm} \right)_{jk} \left(R_L^{\pm\pm} \right)_{lk} &= \text{diag} \left(m_3^{\pm\pm}, m_4^{\pm\pm} \right), \\
\left(R^\pm \right)_{ij} \left(M^\pm \right)_{jk} \left(R^\pm \right)_{lk} &= \text{diag} \left(m_1^\pm, \dots, m_6^\pm, 0, 0 \right), \\
\left(R_s^0 \right)_{ij} \left(M_s^0 \right)_{jk} \left(R_s^0 \right)_{lk} &= \text{diag} \left(m_{s1}^0, \dots, m_{s8}^0 \right), \\
\left(R_p^0 \right)_{ij} \left(M_p^0 \right)_{jk} \left(R_p^0 \right)_{lk} &= \text{diag} \left(m_{p1}^0, \dots, m_{p6}^0, 0, 0 \right)
\end{aligned} \tag{18}$$

where m_{s1} is the mass of the lightest Higgs scalar. Diagonalizing the scalar mass matrices, we introduce new fields by:

$$\begin{aligned}
y_{Ri}^{\pm\pm} &= \left(R_R^{\pm\pm} \right)_{ij} x_{Rj}^{\pm\pm}, \quad y_{Li}^{\pm\pm} = \left(R_L^{\pm\pm} \right)_{ij} x_{Lj}^{\pm\pm}, \quad y_i^\pm = \left(R^\pm \right)_{ij} x_j^\pm, \\
y_{si}^0 &= \left(R_s^0 \right)_{ij} x_{sj}^0, \quad y_{pi}^0 = \left(R_p^0 \right)_{ij} x_{pj}^0
\end{aligned} \tag{19}$$

5.4 Couplings

Finally, we list the all couplings involving doubly charged higgsinos relevant for the production and decay:

$$\tilde{\Delta}_R^{--} \Delta_R^{--} \chi_k^0 \quad \left(\frac{e}{\sqrt{\cos 2\theta_W}} N_{k1} + g N_{k3} \right) P_R \quad (20)$$

$$\tilde{\Delta}_L^{--} \Delta_L^{--} \chi_k^0 \quad \left(\frac{e}{\sqrt{\cos 2\theta_W}} N_{k1} + g N_{k2} \right) P_L \quad (21)$$

$$\tilde{\Delta}_R^{--} \Delta_{Rj}^- \chi_k^- \quad g U_{k2} A_{j7} P_R \quad (22)$$

$$\tilde{\Delta}_L^{--} \Delta_{Lj}^- \chi_k^- \quad g U_{k2} A_{j1} P_L \quad (23)$$

$$\tilde{\Delta}_R^{--} \tilde{l}_R^- l_R^- \quad -2h_u \mathcal{C}^{-1} P_R \quad (24)$$

$$\tilde{\Delta}_L^{--} \tilde{l}_L^- l_L^- \quad -2h_u \mathcal{C}^{-1} P_L \quad (25)$$

where A_{ij} is the matrix which diagonalizes the mass matrix for the singly-charged Higgs bosons. \mathcal{C} is the charge conjugation operator while P_L and P_R are the chirality projection operators $(1 \mp \gamma_5)/2$.

References

- [1] S. Eidelman *et al.* [Particle Data Group], Phys. Lett. B **592** (2004) 1.
- [2] D. N. Spergel *et al.* [WMAP Collaboration], Astrophys. J. Suppl. **148**, 175 (2003).
- [3] R. Barbier *et al.*, Phys. Rept. **420** (2005) 1.
- [4] R. N. Mohapatra and G. Senjanovic, Phys. Rev. Lett. **44**, 912 (1980); R. N. Mohapatra and G. Senjanovic, Phys. Rev. D **23**, 165 (1981); M. Gell-Mann, P. Ramond, R. Slansky, Supergravity (P. van Nieuwenhuizen et al. eds.), North Holland, Amsterdam, 1980, p. 315; T. Yanagida, in Proceedings of the Workshop on the Unified Theory and the Baryon Number in the Universe (O. Sawada and A. Sugamoto, eds.), KEK, Tsukuba, Japan, 1979, p. 95. S.L. Glashow, The future of elementary particle physics, in Proceedings of the Summer Institute on Quarks and Leptons (M. Levy et al eds.), Plenum Press, New York, 1980, pp. 687.
- [5] M. Cvetič and J. Pati, Phys. Lett. B **135**, 57 (1984); R. N. Mohapatra and A. Rašin, Phys. Rev. D **54**, 5835 (1996); R. Kuchimanchi, Phys. Rev. Lett. **76**, 3486 (1996); R.

- N. Mohapatra, A. Rašin and G. Senjanović, Phys. Rev. Lett. **79**, 4744 (1997); C. S. Aulakh, K. Benakli and G. Senjanović, Phys. Rev. Lett. **79**, 2188 (1997); C. S. Aulakh, A. Melfo and G. Senjanović, Phys. Rev. D **57**, 4174 (1998).
- [6] D. A. Demir, M. Frank and I. Turan, Phys. Rev. D **73**, 115001 (2006).
- [7] R. M. Francis, M. Frank and C. S. Kalman, Phys. Rev. D **43**, 2369 (1991); K. Huitu and J. Maalampi, Phys. Lett. B **344**, 217 (1995); K. Huitu, J. Maalampi and M. Raidal, Phys. Lett. B **328**, 60 (1994); K. Huitu, J. Maalampi and M. Raidal, Nucl. Phys. B **420**, 449 (1994).
- [8] R. N. Mohapatra and A. Rasin, Phys. Rev. Lett. **76**, 3490 (1996); R. N. Mohapatra and A. Rasin, Phys. Rev. D **54**, 5835 (1996); R. Kuchimanchi, Phys. Rev. Lett. **76**, 3486 (1996).
- [9] Z. Chacko and R. N. Mohapatra, Phys. Rev. D **58**, 015003 (1998); B. Dutta and R. N. Mohapatra, Phys. Rev. D **59**, 015018 (1999).
- [10] G. Barenboim, K. Huitu, J. Maalampi and M. Raidal, Phys. Lett. B **394**, 132 (1997).
- [11] K. Huitu, J. Maalampi, A. Pietila and M. Raidal, Nucl. Phys. B **487**, 27 (1997).
- [12] K. Huitu, J. Maalampi and M. Raidal, HU-SEFT-I-1995-1, 1995; M. Frank, Phys. Rev. D **62**, 053004 (2000).
- [13] M. Raidal and P. M. Zerwas, Eur. Phys. J. C **8**, 479 (1999).
- [14] M. Singer, J. W. F. Valle and J. Schechter, Phys. Rev. D **22**, 738 (1980); J. C. Montero, F. Pisano and V. Pleitez, Phys. Rev. D **47**, 2918 (1993); P. H. Frampton, Phys. Rev. Lett. **69**, 2889 (1992); R. Foot, O. F. Hernandez, F. Pisano and V. Pleitez, Phys. Rev. D **47**, 4158 (1993); R. Foot, H. N. Long and T. A. Tran, Phys. Rev. D **50**, 34 (1994); J. C. Montero, F. Pisano and V. Pleitez, Phys. Rev. D **47**, 2918 (1993); H. N. Long, Phys. Rev. D **54**, 4691 (1996).
- [15] M. L. Swartz, Phys. Rev. D **40** (1989) 1521; J. F. Gunion, J. Grifols, A. Mendez, B. Kayser and F. I. Olness, Phys. Rev. D **40** (1989) 1546; M. Lusignoli and S. Petrarca, Phys. Lett. B **226** (1989) 397;

- [16] L. Willmann *et al.*, Phys. Rev. Lett. **82** (1999) 49 [arXiv:hep-ex/9807011]; D. Chang and W. Y. Keung, Phys. Rev. Lett. **62** (1989) 2583; S. Godfrey, P. Kalyniak and N. Romanenko, Phys. Rev. D **65** (2002) 033009 [arXiv:hep-ph/0108258].
- [17] G. Abbiendi *et al.* [OPAL Collaboration], Phys. Lett. B **577** (2003) 93 [arXiv:hep-ex/0308052].
- [18] P. Achard *et al.* [L3 Collaboration], Phys. Lett. B **576** (2003) 18 [arXiv:hep-ex/0309076].
- [19] J. Abdallah *et al.* [DELPHI Collaboration], Phys. Lett. B **552** (2003) 127 [arXiv:hep-ex/0303026].
- [20] A. Aktas *et al.* [H1 Collaboration], Phys. Lett. B **638** (2006) 432 [arXiv:hep-ex/0604027].
- [21] R. D. Heuer, Nucl. Phys. Proc. Suppl. **154**, 131 (2006).
- [22] F. Maltoni and T. Stelzer, JHEP **0302**, 027 (2003) [arXiv:hep-ph/0208156].
- [23] M. Frank and P. Pnevmonidis, Phys. Rev. D **67**, 015010 (2003).